Spectral Factor Analysis for Multi–isotope Imaging in Nuclear Medicine

I. Buvat[1], S. Hapdey[1], H. Benali[1], A. Todd-Pokropek[1,2], and R. Di Paola[1]

[1] U494 INSERM, CHU Pitié-Salpêtrière, Paris, France
buvat@imed.jussieu.fr
[2] Department of Medical Physics, University College London, London, UK

Abstract. In nuclear medicine, simultaneous dual-isotope imaging is used to determine the distribution of two radiotracers from a single acquisition and for emission/transmission (E/T) imaging in SPECT. However, no general solution to the cross–talk problem caused by scattered and unscattered photons has been found yet and accurate quantification cannot be performed. We describe a *general* method of spectral factor analysis (SFA) for multi–isotope acquisitions. SFA corrects for cross–talk due to unscattered and scattered photons in planar or SPECT imaging involving two or more radiotracers and for E/T scans. A Tc-99m/I-123 phantom study shows that quantitative accuracy is within 10% with SFA, while errors up to 170% are observed using conventional spectral windows.

1 Introduction

In nuclear medicine, simultaneous dual–isotope imaging is used to determine the distribution of two imaging agents labeled with two different isotopes (e.g., [1,2]) and also for simultaneous emission/transmission (E/T) imaging in SPECT, where one radioisotope is used for transmission scanning while the other is used for the emission study [3]. The major problem with simultaneous dual–isotope acquisition procedure is the cross–talk between the two isotopes. Photons emitted by one radioisotope can be detected in the energy window dedicated to the acquisition of photons emitted by the other and conversely. Cross–talk can be caused by unscattered photons if the photopeaks corresponding to the two radioisotopes partially overlap. Cross–talk is also systematically introduced by scattered photons from the highest energy isotope which are detected in the energy window corresponding to the lowest energy isotope. The magnitude of cross–talk varies with the experimental conditions but it is admitted that the resulting images are not trustworthy without some cross–talk correction [4].

There is currently no method accepted as a standard for cross–talk correction. Symmetrical and off–set energy windows are used (e.g., [1,5]) to reduce cross–talk but do not remove it. Subtraction methods involving at least three energy windows have also been proposed (e.g., [5,6]). However, none of these approaches offers a reliable solution when cross–talk is caused by both scattered

and unscattered photons. In addition, these empirical approaches need substantial changes and specific calibration for each combination of isotopes.

We describe here a general method for the analysis of multi–isotope acquisitions using a spectral factor analysis (SFA). SFA corrects for cross–talk due to both unscattered and scattered photons.

2   Theory

As different radioisotopes can be distinguished by their emission energy spectrum, SFA analyzes the set of spectra detected in the pixels of the planar images (or projections in SPECT), using either a list mode or a multispectral acquisition technique. For the sake of simplicity, we consider here planar imaging (the extension to SPECT is discussed below). A planar acquisition with spectral information consists of a set of E spectral images, each image including photons detected in a small energy interval. $\mathbf{X}_i(e)$ is the number of photons detected in pixel i of image e.

The model assumes that each noise–free spectrum can be written as a linear combination of K spectral components f_k common to all pixels i, i.e.:

$$\mathbf{X}_i(e) = \sum_{k=1}^{K} a_k(i) f_k(e) + \varepsilon_i(e), \tag{1}$$

where $a_k(i)$ is the number of photons in pixel i distributed according to the spectrum f_k and $\varepsilon_i(e)$ represents noise.

For multi–isotope imaging with R isotopes, the spectral components f_k are R scatter–free spectra f_r and $K - R$ scatter spectra. For each isotope r, the $\{a_r(i)\}$ coefficients ($i = 1, \ldots, N$, N is the number of pixels in an image) associated with the scatter–free spectrum f_r give the scatter–free image of isotope r. Solving the model consists in estimating the scatter–free and scatter spectra f_k and the associated $a_k(i)$. This is performed using SFA, derived from the latest developments regarding factor analysis of medical image sequences [7,8]. In the following, we briefly describe the four steps of SFA.

Data preprocessing. First, the spectra corresponding to spatial neighbor pixels are added (e.g., using 4×4 pixel non overlapping ROIs), which is equivalent to a coarse spatial sampling. This reduces the number of spectra to be analyzed and increases the signal–to–noise ratio in each spectrum. Spectra corresponding to irrelevant regions in the images are also discarded, resulting in M spectra $\mathbf{Y}_i$. The model (1) can be written:

$$\mathbf{Y}_i(e) = \sum_{k=1}^{K} a'_k(i) f_k(e) + \varepsilon'_i(e), \tag{2}$$

where the $\{a'_k(i)\}_{i=1,\ldots,M}$ is the image (with coarse sampling) associated with the spectrum f_k and $\varepsilon'_i(e)$ represents noise.

Orthogonal analysis. This stage filters the spectra $\mathbf{Y}_i$, to estimate their noise–free components Y_i assuming these components belong to a low dimensional space S (typically $< 5D$). S is estimated using an orthogonal decomposition adapted to the Poisson nature of the set of spectra $\{\mathbf{Y}_i\}_{i=1,\ldots,M}$, namely a correspondence analysis (CA). CA yields an orthogonal spectral basis from which a Q–dimensional space S, spanned by the Q eigenvectors associated with the largest Q eigenvalues of the covariance matrix decomposed by CA, is obtained [9].

Oblique analysis. The oblique analysis estimates the spectra f_k underlying the model (1) assuming they belong to the subspace S. It is also assumed that the dimension Q of S is equal to the number K of spectra underlying the physical model. To estimate the f_k, a priori knowledge pertaining to the spectra f_k and to the images a'_k must be used [7]. We know that $f_k(e) \geq 0$ and $a'_k(i) \geq 0$ since they represent numbers of photons. In addition, for each scatter–free spectrum $f_r(e) = 0$ for some energy channels where there is no photopeak. Using this information, the R scatter–free spectra f_r are first located in S using the target apex–seeking (TAS) method [10]. Next, the $K - R$ scatter spectra f_k are estimated iteratively by minimizing the number of negative $f_k(e)$ and $a'_k(i)$ values while taking into account the confidence interval around each estimated $f_k(e)$ or $a'_k(i)$ [8].

Oblique projection. An oblique projection finally determines the coefficients $a_k(i)$ of equation (1) given the original spectra $\mathbf{X}_i$ and the estimated spectra f_k [8]. The set of coefficients $\{a_r(i)\}_{i=1,\ldots,N}$ corresponding to the scatter–free spectrum f_r gives the scatter–free image of the isotope r.

3   Material and Methods

The phantom (Fig. 1) consisted of 2 series of 9 overlapping Petri dishes (?=8.6cm, 1.3 cm thick), including various mixtures of I–123 (emission energy of 159 keV) and Tc–99m (emission energy of 140 keV) in water (Table 1).
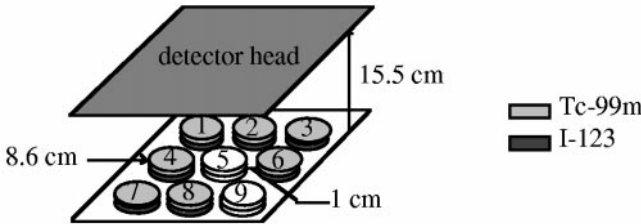

Fig. 1. Phantom used for the acquisition

A planar view of the phantom gave an image of 9 dishes with variable mixtures of Tc–99m and I–123. The total Tc–99m and I–123 activities were 23.1 and 24.8 GBq respectively. A 20 min acquisition (6.45 million counts) was performed on a Elscint Helix gamma camera, equipped with a low energy high resolution

collimator, using 32 spectral images (3.5 keV wide each) with a matrix 256×256 (pixel size = 1.47 mm) between 63 and 175 keV.

Table 1. Percentages of Tc–99m and I–123 activity in each dish of the phantom

dish number	1	2	3	4	5	6	7	8	9
percentage of Tc–99m	36	32	22.6	15	0	68.3	83.5	89.7	0
percentage of I–123	64	68	77.4	85	0	31.7	16.5	10.3	0

The resulting 32 images were processed using SFA: 8×8 pixel grouping, TAS of the Tc–99m photopeak assuming it was zero between 63 and 126 keV and between 154 and 175 keV and TAS of the I–123 photopeak assuming it was zero between 63 and 143.5 keV. A scatter spectrum was estimated using non–negativity constraints only. The SFA cross–talk free images were compared to the Tc–99m and I–123 images obtained using "optimal" energy windows [11]: a 15% window centered on 140 keV (129.5–150.5 keV) for Tc–99m and a 154–175 keV window for I–123 (called WIN images below).

The Tc–99m and I–123 images were analyzed by drawing circular ROIs inside each dish (?=4.5 cm). The mean number of counts inside each ROI was calculated. Using the Tc-99m (resp. I–123) image, the dish with the largest mean number of counts N_{Tcmax} (resp. N_{Imax}) was identified and, for each dish d, the ratio of the mean number of counts $N_{\text{Tc-d}}$ (resp. $N_{\text{I-d}}$) in the dish d to N_{Tcmax} (resp. N_{Imax}) was determined. These ratios $N_{\text{Tc-d}}/N_{\text{Tcmax}}$ and $N_{\text{I-d}}/N_{\text{Imax}}$ represent the activity ratios (AR) between different regions in the Tc–99m and I–123 images. In each dish d, the AR $N_{\text{Tc-d}}/N_{\text{I-d}}$ was also determined. All AR were compared to their true values theoretically derived given the real activity in the dishes and the attenuation effect. As this was planar imaging, no absolute quantitation was attempted.

4   Results

The spectra (Fig. 2) estimated using SFA and the location of the spectral windows used for WIN as defined above show that, when using WIN, cross–talk in the Tc–99m window is due to scattered photons and unscattered I–123 photons and that some Tc–99m unscattered photons are outside the Tc–99m window. On the other hand, cross–talk in the I–123 image is mostly due to scattered photons. WIN I–123 window also rejects many I–123 unscattered photons.

Figs. 3a–b show the Tc–99m and I–123 AR measured in the different dishes for the estimated Tc–99m and I–123 images. Using WIN Tc–99m image, errors up to 81% (ROI 3) and 170% (ROI 4) were observed for low $N_{\text{Tc-d}}/N_{\text{Tcmax}}$ values (22.5 and 11.0% respectively). With the SFA Tc–99m image, the largest errors observed for $N_{\text{Tc-d}}/N_{\text{Tcmax}}$ AR were 4.4% and 5.8% for ROIs 6 and 8 where the true AR were 73.2% and 87.8% respectively.

The differences in performance between the methods where less obvious for the I–123 images, with errors between 1.5% (ROI 6) and 9.7% (ROI 5) for WIN,
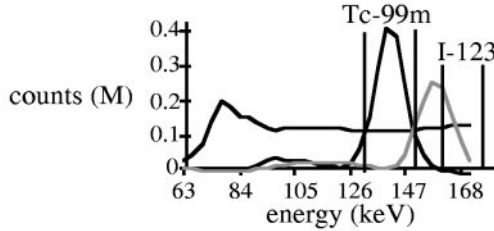
Fig. 2. Spectra estimated using SFA and spectral windows used in WIN

and between 0.8% (ROI 9) and 9.3% (ROI 7) for SFA. The I–123 AR measured in cold dishes 5 and 9 were $< 1.5\%$ with SFA and they were between 4.5 and 11.8% with WIN.
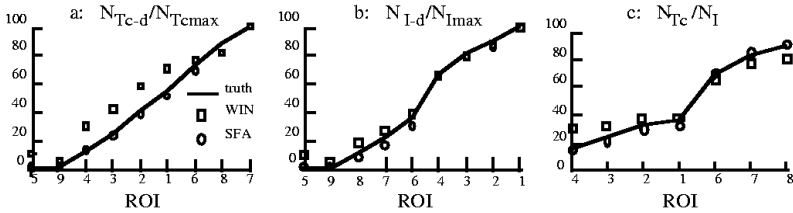

Fig. 3. Relative quantitation results from the WIN and SFA Tc–99m and I–123 images

Fig. 3c shows the estimated N_{Tc-d}/N_{I-d} AR, the WIN images yielded an overestimation of the AR for the lowest AR and an underestimation for the highest AR, with errors between +13.9% (ROI 4) and -9% (ROI 8). SFA images gave errors between -1.5% (ROI 7) and +4.4% (ROI 1).

5   Discussion and Conclusion

Simultaneous dual–isotope studies are currently hindered by cross–talk problems, for which there are no satisfactory solutions yet [4]. The SFA method offers a general solution, since it can be used a priori for any radioisotope combination, both for studies involving two radiopharmaceuticals and for E/T studies. SFA is a data driven approach and the severity of cross–talk does not have to be known a priori. However, as the linear model underlying SFA is quite general, a priori knowledge must be used to find the solution appropriate to the physics of the problem. This a priori knowledge relates to the energy range in which the photopeaks should be zero and does not have to be extremely precise: a change of few keV in the definition of this energy range (up to 10 in our example) did not affect the results. SFA corrects for cross–talk due to scattered and unscattered photons. SFA takes advantage of the Poisson nature of the data when filtering the noise (in the orthogonal analysis) and when estimating the

model components (in the oblique analysis). The method permits a quantitative interpretation of the results, which is of paramount importance for E/T imaging. SFA model is not stationary, i.e. it does not intrinsically assume that the scatter spectrum has the same shape in every pixel. However, estimating at least 4 spectra is needed to make the analysis non stationary. In our example, accurate results were obtained when assuming scatter stationarity (i.e. considering 3 factors only).

The challenging Tc–99m/I–123 phantom we considered showed that SFA outperformed the method using energy windows, which is the only alternative proposed so far for this couple of radioisotopes.

Although we gave evidence that SFA could offer a solution to the cross–talk problem, further investigations involving other combinations of radioisotopes, in emission/emission or E/T studies should now be conducted. So far, only planar images have been processed, but SPECT data can be dealt with similarly using a single SFA of the spectra corresponding to all projections, before reconstruction.

References

1. Devous, M.D., Payne, J.K., Lowe, J.L.: Dual–isotope brain SPECT imaging with Technetium–99m and Iodine–123: clinical validation using Xenon–133 SPECT. J. Nucl. Med. **33** (1992) 1919–1924
2. Schoeder, H., Topp, H., Friedrich, M., Jatzkewitz, A., Roser, M.: Thallium and indium antimyosin dual–isotope single–photon emission tomography in acute myocardial infarction to identify patients at further ischaemic risk. Eur. J. Nucl. Med. **21** (1994) 415–422
3. Bailey, D.L.: Transmission scanning in emission tomography. Eur. J. Nucl. Med. **25** (1998) 774–787
4. Links, J.M.: Simultaneous dual–radionuclide imaging: are the images trustworthy? Eur. J. Nucl. Med. **23** (1996) 1289–1291
5. Ivanovic, M., Weber, D.A., Loncaric, S., Franceschi, D.: Feasability of dual radionuclide brain imaging with I–123 and Tc–99m. Med. Phys. **21** (1994) 667–674
6. Moore, S.C., English, R.J., Syravanh, C., Tow, D.E., Zimmerman, R. E., Chan, K.H., Kijewski, M.F.: Simultaneous Tc–99m/Tl–201 imaging using energy–based estimation of the spatial distribution of contaminant photons. IEEE Trans. Nucl. Sci. **42** (1995) 1189-1195
7. Benali, H., Buvat, I., Frouin, F., Bazin, J.P., Di Paola, R.: Foundations of factor analysis of medical image sequences. Image and Vision Computing **12** (1994) 375–385
8. Buvat, I., Benali, H., Di Paola, R.: Statistical distribution of factors and factor images in factor analysis of medical image sequences. Phys. Med. Biol. **43** (1998) 421–434
9. Benali, H., Buvat, I., Frouin, F., Bazin, J.P., Di Paola, R.: A statistical model for the determination of the optimal metric in Factor Analysis of Medical Image Sequences (FAMIS). Phys. Med. Biol. **38** (1993) 1065–1080
10. Buvat, I., Benali, H., Frouin, F., Bazin, J.P., Di Paola, R.: Target apex–seeking in factor analysis of medical image sequences. Phys. Med. Biol. **38** (1993) 123–138
11. Hindié, E., Mellière, D., Jeanguillaume, C., Perlemuter, L., Chéhadé, F., Galle, P.: Parathyroid imaging using simultaneous double–window recording of Technetium–99m–sestamibi and Iodine–123. J. Nucl. Med. **39** (1998) 1100–1105